RSC Advances

ROYAL SOCIETY OF CHEMISTRY

www.rsc.org/advances

Effect of multifunctional samarium lysine dithiocarbamate on curing properties, static and dynamic mechanical properties of SBR/silica composites

Yongkun Zou, Jingwei He, Zhenghai Tang, Lixin Zhu, Yuanfang Luo and Fang Liu*

College of Materials Science and Engineering, Key Lab of Guangdong Province for High Property and Functional Macromolecular Materials, South China University of Technology, Guangzhou, 510640, P. R. China

Corresponding E-mail: mcfliu@126.com   Tel: +86 20 87114857

Abstract

In this work, a novel multifunctional rubber agent named as samarium lysine dithiocarbamate (Sm-LDC) was synthesized by nucleophilic addition reaction and coordination reaction. Then the influences of Sm-LDC on curing property, static and dynamic mechanical properties of SBR/SiO$_2$ composites were studied. The results showed that Sm-LDC is capable to accelerate the vulcanization of SBR compounds even without zinc oxide (ZnO) and stearic acid (SA), and conducive to reinforce crosslink network. Notably, SBR/Sm-LDC/SiO$_2$ composites exhibit superior static and dynamic mechanical properties in comparison with SBR/SiO$_2$ composite containing conventional accelerator zinc diethyl dithiocarbamate (ZDC), activators ZnO and SA. Such improvement is attributable to the improved dispersion of SiO$_2$, the enhanced filler-rubber interaction, and high vulcanization and reinforcing efficiency of Sm-LDC. Accordingly, the excellent comprehensive performance may make Sm-LDC very competitive in the application of green tire and the preparation of high performance rubber composites.

1 Introduction

In recent years, rubber/filler composites are one of the most interesting areas in various

technological applications and fundamental research.[1-6] The introduction of filler, such as carbon

black, silica (SiO_2), montmorillonite and halloysite nanotubes into the rubber is a simple and

effective method to remarkably improve the mechanical properties[7-9] and other unique

performances[10,11] of rubber composites. Among these fillers, SiO_2 has been considered as one of

the most attractive nanofillers and potential alternatives of carbon black in rubber industry because

of the several favorable advantages such as inexpensive, nontoxic and biocompatible. However,

due to the abundant silanol groups on the surface of SiO_2, SiO_2 particles tend to aggregate in the

rubber matrix, leading to poor filler dispersion and weak filler-rubber interaction, which extremely

worsens the performance of rubber/SiO_2 composites. Fortunately, many efforts are underway to

overcome this problem and the surface modification of SiO_2 seems to be a practical and effective

approach.[12-14]

Moreover, it is well known that vulcanization is a necessary process for rubber products to meet

the various demands in practical application and vulcanization systems of the rubber are critical

factors in determining the performance of resulting rubber composites. Conventionally,

vulcanization systems of rubber are consists of activators zinc oxide (ZnO) and stearic acid (SA),

accelerators (dithiocarbamate, thiuram, sulfonamide, benzothiazole, thiourea, etc.) and sulfur.

However, the conventional accelerators and activators can only speed up the vulcanization of

rubber compounds but without any significant effect on filler dispersion and filler-rubber

interaction. Even worse, many conventional accelerators, such as dithiocarbamate, thiuram and

sulfonamide, are derived from secondary amine, which are strictly restricted in European Union

(EU) and USA due to the carcinogenicity of nitrosamine during the vulcanization process.[15] In

addition, about 5 phr (weight parts per 100 weight parts rubber) conventional ZnO are usually

used in the vulcanization. However, the conventional ZnO was classified as a hazardous chemical

in EU and its application in rubber technology should be effectively reduced and controlled.[16]

Therefore, to prepare the environmentally friendly and high performance rubber composites,

developing an efficient and multifunctional agent which can realize the replacement of traditional

toxic accelerators and activators completely, and the improvement of filler dispersion and

filler-rubber interfacial interaction simultaneously is worthy to explore both in academy and in

rubber industry.

In this work, a novel multifunctional rubber agent named samarium lysine dithiocarbamate

(Sm-LDC) was synthesized by nucleophilic addition reaction between carbon disulfide and

primary amine and coordination reaction of samarium ion. Then the resulting multifunctional rare

earth dithiocarbamate was incorporated into styrene butadiene rubber (SBR) matrix and its

influence on the curing property, the static and dynamic mechanical properties of SBR/SiO$_2$

composites was investigated. The dispersion of SiO$_2$ and filler-rubber interfacial interaction was

evaluated by field emission scanning electron microscopy (FESEM) and ammonia modified

toluene equilibrium swelling method, respectively. Besides, the reaction process of sulfur

vulcanization and reinforcement mechanism in SBR/Sm-LDC/SiO$_2$ composites was discussed.

2 Experimental

2.1 Materials

Samarium oxide (Sm$_2$O$_3$, 99%) was kindly provided by GanZhou Xinsheng Rare Earth Industrial

Co., Ltd. Hydrochloric acid (HCl) was obtained from Guangzhou Chemical Reagent Factory.

Lysine (C$_6$H$_{14}$N$_2$O$_2$, 98%) was purchased from J&K Scientific Co., Ltd. Sodium hydrate (NaOH)

and carbon disulfide (CS$_2$) were purchased from Tianjin Fuchen Chemical Reagent Factory. All

chemicals used in the synthesis of Sm-LDC were of analytical grade and used as received.

Styrene-butadiene rubber (SBR-1502, styrene content of 25%), precipitated silica (SiO_2) and rubber additives such as activators zinc oxide (ZnO) and stearic acid (SA), accelerator zinc diethyl dithiocarbamate (ZDC), accelerator 2,2'-benzothiazole disulfide (DM) and sulfur (S) were kindly supplied by Dongguan First Rubber & Plastic Technology Co., Ltd. All rubber additives were of industrial grade and used as received.

2.2 Synthesis of Sm-LDC

The synthesis route of Sm-LDC is displayed in Fig. 1. 2.92 g of lysine and 2.40 g of NaOH were added into a three necked flask with magnetic stirring and 50 ml of deionized water. The mixture was stirring until become clear solution. Then 3.04 g of CS_2 was slowly dropped into the aforementioned clear solution using a constant pressure drop funnel under ice bath conditions. The mixture was stirring for 2 h at 45 °C for reaction to get Na-LDC. Then Na-LDC aqueous solution was mixed with as-prepared samarium chloride aqueous solution in a stoichiometric level with continuous stirring for 2 h at 45 °C. The precipitation product was filtered out and washed by deionized water (4 times). At last, the precipitation product was dried under vacuum at the temperature of 40 °C to get a hoar powder. The yield of the final target product Sm-LDC is 65.1%.

2.3 Preparation of unfilled SBR and SBR/SiO₂ composites

The SBR/Sm-LDC and SBR/Sm-LDC/SiO_2 composites were prepared following the formulations given as follows: SBR, 100 phr; SiO_2, 0 phr (unfilled) or 30 phr (filled); Sm-LDC, variable; DM, 1.0 phr; sulfur, 2.0 phr. First, SBR was passed through the roller three times on an open two-roll mill at room temperature with the nip gap of about 1 mm and the rotors were operated at a speed ratio of 1(front): 1.22 (back), then SiO_2 and the ingredients, such as Sm-LDC (or ZnO, SA, ZDC),

DM and S, were added to the glue stock one by one within 10 min. After placing at room temperature for 12 h, SBR compounds were vulcanized in an electrically heated press at 160 ºC according to their optimum vulcanization time (Tc_{90}) which was previously determined by an UR-2050 ODR instrument. To investigate the influence of Sm-LDC on the curing property and mechanical performance of unfilled SBR and SBR/SiO_2 composites, a series of unfilled SBR and SBR/SiO_2 composites were prepared containing up to 1.0, 2.0, 4.0, 6.0 and 8.0 phr of Sm-LDC. For convenience, these vulcanizates of unfilled SBR and SBR/SiO_2 composites are abbreviated as "Sm-LDC-x" and "SiO_2/Sm-LDC-x", respectively. The unknown number x denotes Sm-LDC content (phr) in the vulcanizates. For comparison, the unfilled SBR and SBR/SiO_2 vulcanizates with activators ZnO (5.0 phr), SA (2.0 phr) and conventional dithiocarbamate accelerator ZDC (2.0 phr) were also prepared by the identical procedure, which are coded as "Sm-LDC-0" and "SiO_2/Sm-LDC-0", respectively.

2.4 Preparation of Sm-LDC/SiO_2 model compounds

To shed light on the interactions between Sm-LDC and SiO_2 more clearly, Sm-LDC and SiO_2 powder were employed to prepare the Sm-LDC/SiO_2 model compounds. The samples of Sm-LDC, SiO_2 and Sm-LDC/SiO_2 model compounds were prepared by a vulcanizing press machine at a setting time of 20 min under 160 ºC using Sm-LDC, SiO_2, and the mixture of Sm-LDC and SiO_2 powders, respectively. Then, the analysis of interactions between Sm-LDC and SiO_2 were performed by Fourier transform infrared spectra (FT-IR) and X-ray photoelectron spectroscopy (XPS).

2.5 Characterization and Measurement

2.5.1 Structural characterization of Sm-LDC

Ultraviolet-Visible (UV-Vis) absorption spectra of lysine and Na-LDC aqueous solution with a concentration of 1 mmol/L were carried out on the UV-4802 UV-Vis absorption spectrum analyzer (Unico Co USA) from 200 nm to 600 nm with the speed of 600 nm / min.

Nuclear Magnetic Resonance spectrum (^{13}C-NMR) of Na-LDC (D_2O as solvent) was measured on Bruker-600 MHz nuclear magnetic resonance instrument.

Fourier transform infrared (FT-IR) spectra of Lysine, Na-LDC, Sm-LDC and the samples of Sm-LDC, SiO_2 and Sm-LDC/SiO_2 model compounds were recorded with a Vector33 FT-IR spectrometer (Bruker, German) from 400 cm^{-1} to 4000 cm^{-1} by using the KBr disc method.

X-ray photoelectron spectroscopy (XPS) of Na-LDC, Sm-LDC and the samples of Sm-LDC, SiO_2 and Sm-LDC/SiO_2 model compounds were recorded by using an X-ray photoelectron spectrometer (PHI X-tool) with an Al Kα (mono) source. The Al Kα (mono) source was operated at 15 kV and 51W. The treatments of high-resolution survey of the samples were performed with XPS Peak 4.1 software.

Elemental analysis of Sm-LDC was carried out on a Vario EL Elemental analyzer (ELEMENTAR Co, Germany).

2.5.2 Curing properties

Curing studies of un-vulcanized rubber compounds were carried out by using an ODR instrument (U-CAN UR-2050, Taiwan) with an amplitude of ± 1° and a frequency of 1.66 Hz for all the samples at 160 ºC for 40 minutes.

2.5.3 Crosslink density

Crosslink density of vulcanizates was determined by ammonia modified toluene equilibrium swelling method. Samples were immersed in toluene at the ammonia atmosphere for 5 days and

then removed from the solvent and the surface toluene was blotted off quickly with tissue paper. The specimens were immediately weighed and then dried in a vacuum oven until the samples had constant weight and was reweighed. The volume fraction of SBR in the swollen gel, V_r, was calculated by the following equation suggested by Flory-Rhener[17]:

$$V_r = \frac{m_0 \phi (1-\alpha)/\rho_r}{m_0 \phi (1-\alpha)/\rho_r + (m_1 - m_2)/\rho_s}$$ (1-1)

where m_0 is the sample mass before swelling, m_1 and m_2 are sample masses before and after drying, respectively, ϕ is the mass fraction of rubber in the vulcanizate, α is the mass loss of the gum SBR vulcanizate during swelling, and ρ_r and ρ_s are the rubber and solvent density, respectively.

The crosslinking density of the vulcanizate, V_e, was then calculated by the following equation[18]:

$$V_e = -\frac{\ln(1-V_r) + V_r + \chi V_r}{V_s (V_r^{1/3} - V_r/2)}$$ (1-2)

where V_r is the volume fraction of the polymer in the vulcanizate swollen to equilibrium and V_s is the solvent molar volume (107 cm^3/mol for toluene). χ is the SBR-toluene interaction parameter and is taken as 0.0653 calculated according to reference[19]. To reduce the random error, five specimens for each vulcanizate were employed to the measurement and the crosslink density of each vulcanizate was acquired by the average value of their five samples.

2.5.4 Morphology

Morphology of fracture surfaces of samples were examined by field emission scanning electron microscopy (FESEM, NOVA NANOSEM 430) at the acceleration voltage of 5 kV.

2.5.5 Mechanical properties

Mechanical performances including tensile and tear properties were performed using a universal testing machine (U-CAN UT-2060, Taiwan) with a cross-head speed of 500 mm/min

according to the respective standards ISO 37: 2011 and ISO 34-1: 2010. Shore A hardness was

measured according to standard ISO 7619-1: 2010.

2.5.6 Dynamic mechanical properties

Dynamic mechanical analysis (DMA) of SBR/Sm-LDC/SiO$_2$ composites and

SBR/Sm-LDC-0/SiO$_2$ was investigated by a dynamic mechanical analyzer (DMA242C,

NETZSCH, Germany) using a rectangle sample strip with the size of 8 mm × 6 mm × 1 mm

(length, width, thickness) at the tension model. All tests were conducted at the frequency of 1 Hz

and the amplitude of 10 μm from -100 ºC to 80 ºC with the heating rate of 3 ºC/min.

3 Results and discussion

3.1 Structural characterization of Sm-LDC

UV-Vis absorption spectrum and ^{13}C-NMR spectrum are important methods to characterize the

chemical composition and the molecular structure. Results of UV-Vis absorption spectra of Lysine,

Na-LDC are illustrated in Fig. 2a. Compared with Lysine, two new absorption peaks located at

254, 286 nm can be obviously observed for Na-LDC. The two absorption peaks belong to the

transition of $\pi \rightarrow \pi^*$ and $n \rightarrow \pi^*$, respectively, which was derived from the group of NCS$_2$[20,21]. This

result shows that the carbon disulfide successfully reacts with primary amine groups of lysine. In

order to investigate the detail molecular structure of Na-LDC, the ^{13}C-NMR spectrum was carried

out as shown in Fig. 2b. Eight kinds of carbon atoms can be found in the chemical structure of

Na-LDC in total and each carbon atom has the only corresponding chemical shift[22] (C$_1$: 209.9 ppm,

C$_2$: 48.0 ppm, C$_3$: 27.7 ppm, C$_4$: 22.8 ppm, C$_5$: 34.5 ppm, C$_6$: 63.0 ppm, C$_7$: 183.4 ppm, C$_8$: 210.8

ppm), further demonstrating that the intermediate product Na-LDC has been synthesized

successfully as designed in Fig. 1.

8

To investigate the chemical change of Lysine during its chemical reaction, the FT-IR spectra of Lysine, Na-LDC and Sm-LDC were recorded. As shown in Fig. 2c, it is obvious that a new peak appears at 963 cm^{-1} which belongs to symmetric stretching vibration band of dithiocarboxyl group.[23] In addition, the peak of primary amine groups at 3421 cm^{-1} in Lysine shifts to 3374 cm^{-1} in Na-LDC and the asymmetric and symmetric stretching vibration of carbonyl in Lysine shift from 1574 cm^{-1} and 1410 cm^{-1} to 1580 cm^{-1} and 1416 cm^{-1} in Na-LDC, respectively. All these evidences deeply confirm that the carbon disulfide chemically reacts with primary amine groups of Lysine which is highly consistent with the aforementioned results of UV-Vis absorption spectrum and ^{13}C-NMR spectrum. Compared with Na-LDC, the symmetric stretching vibration band of dithiocarboxyl group shifts to 972 cm^{-1} and the asymmetric stretching vibration peak and symmetric stretching vibration peak of carbonyl group appear in 1584 cm^{-1} and 1418cm^{-1} when the thio-carboxyl and carboxyl are chelated with the samarium ions, suggesting that the rare earth atom has replaced the sodium ions of Na-LDC and generated the chelate bond of Sm-O and Sm-S. It should be noted that the peaks situated at 3445 cm^{-1} and 1636 cm^{-1} is assigned to the stretching vibration and bending of hydroxyl of bound water,[2,4] respectively, which indicates that bound water is a part of the molecular structure of Sm-LDC.

To further demonstrate the difference chemical bonding of the metal ions and the carboxyl and dithiocarboxyl groups in Na-LDC and Sm-LDC, XPS is applied to investigate the binding energy of Na-LDC and Sm-LDC. The whole XPS spectra are shown in Fig. 2d and high-resolution survey of S and O are displayed in Fig. 2e and 2f, respectively. In Fig. 2d, the binding energy peaks of metallic samarium ion were appeared in Sm-LDC while not in Na-LDC, which reveals the existence of metallic samarium ion in Sm-LDC. In Fig. 2e and 2f, it could be observed that the

increment of binding energies of sulfur atom in the Sm-LDC are 0.4 eV and 0.6 eV, respectively, compared to that in the Na-LDC. Also, the binding energies of oxygen atom in the Sm-LDC are 0.3 eV and 0.4 eV higher than that in the Na-LDC, respectively. The increment of the binding energy of sulfur atom and oxygen atom provides clear proof that the chemical bonds between the samarium ion and the carboxyl and dithiocarboxyl groups are more stronger than with sodium ion which may be caused by the greater electro-negativity of samarium ion and the stronger bi-dentate chelate bond between the samarium ion and the carboxyl and dithiocarboxyl groups. Moreover, a new binding energy of oxygen atom appears in the Sm-LDC, which may originate from the bound water in the Sm-LDC. Furthermore, elemental analysis is an effective way to determine the element content in the compound. As summarized in Table 1, it could be seen that experimental values of carbon, nitrogen and hydrogen content of Sm-LDC quite consistent with the theoretical value of Sm-LDC. Combining with the analysis of those dates, one may expect that the chemical formula of Sm-LDC is $SmC_8H_{11}N_2O_2S_4 \cdot 2H_2O$ and the possible chemical structure of Sm-LDC is displayed in Fig. 1.

3.2 Interactions analysis of Sm-LDC and SiO_2

FTIR is an effective method to investigate the existence of interactions such as hydrogen bonding and coordination bond.[24,25] The FTIR spectra of SiO_2, Sm-LDC and Sm-LDC/SiO_2 model compounds are shown in Fig. 3a. An obvious red shift in the stretching vibration of O-H group of the SiO_2 from 3442 cm^{-1} to 3376 cm^{-1} in the Sm-LDC/SiO_2 model compound can be observed from Fig. 3a, which is attributed to the formation of hydrogen bond between carboxyl group of Sm-LDC and O-H group of the SiO_2. The asymmetric and symmetric stretching vibration of carbonyl group in the Sm-LDC model compound were located in 1574 cm^{-1} and 1418 cm^{-1},

respectively, which are blue-shifted to 1580 cm^{-1} and 1422 cm^{-1} in the Sm-LDC/SiO$_2$ model

compound, indicating that the chemical environment of the carboxyl group has changed. The

FTIR results of the Sm-LDC/SiO$_2$ model compound illuminate that hydrogen bonds have been

formed between carboxyl of Sm-LDC and the silanol groups of SiO$_2$. Also, these shifts in the

bending vibration and the symmetrical stretching vibration of Si-O bond which evolves from 472

cm^{-1} and 800 cm^{-1} of SiO$_2$ to 476 cm^{-1} and 806 cm^{-1} of the Sm-LDC/SiO$_2$ model compound gives a

hint for the formation of Sm-O coordination bond.

To further determine the formation of coordination bond between SiO$_2$ and Sm-LDC, XPS

analysis was carried on the model compounds. The XPS results are displayed in Fig. 3b and 3c. It

is well known that the chemical environment of the atoms will be influenced by the formation of

coordination bond, which can be revealed by the variation of binding energy of the atoms related

to the coordination bond. As displays in Fig. 3b, the increment of binding energies of samarium

atom in the Sm-LDC/SiO$_2$ powder are 0.3 eV and 0.2 eV, respectively, compared to that of the

Sm-LDC powder, providing convincing proof for the formation of coordination bond of samarium

cation.[26] Meanwhile, the binding energy of Si2p for SiO$_2$ is situated at 102.9 eV, which is ascribed

to the O-Si-O bond[27]. Apparently, in the case of Sm-LDC/SiO$_2$, the binding energy for O-Si-O

bond is located at 103.1 eV, which further demonstrates the existence of hydrogen bond. Moreover,

a new binding energy of silicon for Sm-LDC/SiO$_2$ appears at 103.9 eV, indicating the existence of

coordination bond. Accordingly, it can reasonably be concluded that hydrogen bond and

coordination bond have been formed in the Sm-LDC/SiO$_2$ model compound as other researchers

described.[28]

3.3 Curing behavior of unfilled SBR and SBR/SiO$_2$ compounds

The curing properties of rubber compounds are crucial to prepare high performance rubber/filler composites. In order to study the effect of Sm-LDC on curing properties of unfilled SBR and SBR/SiO$_2$ system, ODR instrument was utilized to give a survey on the curing behavior of SBR/Sm-LDC and SBR/Sm-LDC/SiO$_2$ compounds, as well as the unfilled SBR and SBR/SiO$_2$ compounds containing 5 phr ZnO, 2 phr SA and 2 phr ZDC. The curing properties of unfilled SBR and SBR/SiO$_2$ compounds are assessed by the parameters of scorch time (Ts$_2$), optimum curing time (Tc$_{90}$), minimum torque (M$_L$), and maximum torque (M$_H$). As displayed in Fig. 4a, a consistent decrease in Ts$_2$ and Tc$_{90}$ with increasing Sm-LDC content can be observed in both SBR/Sm-LDC and SBR/Sm-LDC/SiO$_2$ system, which indicates that Sm-LDC can expedite the vulcanization of unfilled SBR and SBR/SiO$_2$ system. Meanwhile, it is accepted that cure rate index (CRI = $100/(Tc_{90}-Ts_2)$) can be used to evaluate the vulcanization rate, where higher vulcanization rate leads to higher value of CRI. As shown in Fig. 4c, the CRI of SBR/Sm-LDC and SBR/Sm-LDC/SiO$_2$ compounds increase monotonously with the increase of Sm-LDC. This further demonstrates that Sm-LDC can effectively accelerate the sulfur crosslink reaction of SBR/Sm-LDC and SBR/Sm-LDC/SiO$_2$ compounds even without activator ZnO and SA. Comparing with unfilled SBR, the Ts$_2$ monotonically decreases for SBR/SiO$_2$ compounds at corresponding Sm-LDC loading while the Tc$_{90}$ goes higher. However, it seems that a decelerating effect is found in SiO$_2$ filled rubber compounds according to the CRI. This may be result from the adsorption effect of SiO$_2$ on vulcanization accelerator, thereby hindering the vulcanization of rubber.[29] Moreover, it is worth noting that the vulcanization characteristics of SBR/Sm-LDC and SBR/Sm-LDC/SiO$_2$ compounds with 6 phr Sm-LDC are comparable to those with 5 phr ZnO, 2 phr SA and 2 phr ZDC. Furthermore, it can be seen that the M$_L$ of SBR/Sm-LDC and

12

SBR/Sm-LDC/SiO$_2$ compounds remain nearly unchanged with increasing Sm-LDC but higher

than those of unfilled SBR and SBR/SiO$_2$ compounds with ZnO, SA and ZDC as depicted in Fig.

4b. However, M$_H$ and the difference between M$_H$ and M$_L$ (ΔM), closely related to the crosslink

density, increases to the maximum value and then decreases with the further addition of Sm-LDC

in SBR/Sm-LDC system, whereas the upward trend for M$_H$ and ΔM is observed in

SBR/Sm-LDC/SiO$_2$ system as shown in Fig. 4b and 4c. This phenomenon strongly suggests that

the types of crosslink density in SBR/Sm-LDC/SiO$_2$ system may differ from that of SBR/Sm-LDC

system.

3.4 Crosslink density of SBR/Sm-LDC/SiO$_2$ composites

To investigate the influence of Sm-LDC and SiO$_2$ on the types of crosslink density and

filler-rubber interaction, the ammonia modified toluene swelling equilibrium method was adopted.

Some researchers[30, 31] proposed that it contained three types of crosslinks in rubber/SiO$_2$

composites, namely, simple rubber-filler absorption bond, rubber-filler hydrogen adhesive bond

and chemical bond or coordination bond. For the first two type bonds, they could be dissociated

by ammonia modified toluene swelling equilibrium via surrounding a papery molecule layer

between the surface of filler and rubber molecule chain and the nitrogen donated atom of

ammonia molecule coordinated with hydrogen atom on the surface of fillers, respectively.

However, the third type bond, chemical bond or coordination bond, would not suffer from

ammonia modified toluene swelling equilibrium. Hence, the crosslink density obtained by

ammonia modified toluene swelling equilibrium is the actual chemical crosslinking density.

Moreover, the difference of the actual chemical crosslinking density between unfilled rubber

vulcanizates and filled rubber vulcanizates V_c is the chemical crosslinking of filler-rubber

interaction which can be used to appraise the intensity of interfacial interaction between filler and rubber. As summarized in Fig. 5a, An interesting result is found that the crosslink density of the SBR/Sm-LDC/SiO$_2$ composites are higher than that of SBR/Sm-LDC vulcanizates at the same loading of Sm-LDC, and an inverse trend is observed between SBR/Sm-LDC-0/SiO$_2$ composite and SBR/Sm-LDC-0 vulcanizate. Moreover, the chemical crosslinking density of filler-rubber interaction (V_c) in SBR/Sm-LDC-0/SiO$_2$ composite is a negative value, while those of SBR/Sm-LDC/SiO$_2$ composites are positive and increases with the increasing Sm-LDC content as shown in Fig. 5b, indicating that a different interfacial interaction mechanism existed in the two different curing systems. Generally, the obstructed effect and surface absorbed accelerator effect of inorganic filler would give rise to a decline in the crosslinking density of filled rubber vulcanizates such as SBR/Sm-LDC-0/SiO$_2$ composite. However, the opposite result occurs in the SBR/Sm-LDC/SiO$_2$ composites, indicating the reaction among rubber chains, Sm-LDC and SiO$_2$ particles contributes a positive value for chemical crosslink.

Combined with the curing data above, a possible reaction process of vulcanization in SBR/Sm-LDC/SiO$_2$ compounds is illustrated in Fig. 6 according to other researchers' investigations.[32-37] The samarium ion catalyzes the reaction between the vulcanization precursor form (A) and Sm-LDC (B) due to the magical 4f and 3d electron orbits, results of which generate another extremely active precursor (C). Then precursor (C) substitutes the alkyl hydrogen atom of the rubber chain and the sulfur crosslink (D) is formed, simultaneously, the two dithiocarboxyl groups of Sm-LDC can completely or partly graft into rubber chain, forming the corresponding crosslink network (E) and pendent groups on the rubber chains (G), respectively. Additionally, the carboxyl group and samarium ion of the multi-functional accelerator Sm-LDC can react with the

14

abundant silanol groups on the surface of SiO_2 particles via hydrogen bonding and coordination

bonding as demonstrated in Fig. 2. Hence, a possible structure of chemical crosslink network[37,38]

would form in the SBR/Sm-LDC/SiO_2 composites as proposed in Fig. 7. It should be noted that, in

the SBR/Sm-LDC/SiO_2 composites, the SiO_2 particles become additional chemical junction due to

the grafting reaction of dithiocarboxyl group and the interaction between SiO_2 particles and

Sm-LDC. However, the SiO_2 particles hinder the formation of the crosslinking network in

SBR/Sm-LDC-0/SiO_2 composites. Furthermore, the Sm-LDC molecule may resemble as the

poly-sulfur bond due to its length and softness, and also acts as a bridge between the rubber matrix

and SiO_2 particles. Such results construct the more complex crosslinking network and enhance the

filler-rubber interfacial adhesion.

3.5 Morphological analysis of SBR/SiO_2 composites

The field emission scanning electron microscopy (FESEM) is a powerful tool for analyzing the

inter-phase morphology and dispersion of filler in polymer/filler composites. Fig. 8a and 8g shows

FESEM image of the fracture surface morphology and EDS spectra corresponding to the

circle-marked region of SBR/Sm-LDC-0/SiO_2 composite, respectively. As shown in Fig. 8a and

8g, many SiO_2 agglomerates are observed because of the strong hydrogen bonds between the

hydroxyl groups on their surface. Besides, it is observed that some residual ZnO particles exist in

the matrix without participating in the vulcanization. For SBR/Sm-LDC/SiO_2 composites, few of

SiO_2 agglomerates appear in SBR matrix with low Sm-LDC content as exhibited in Fig. 8b and 8c.

It can be seen that the SiO_2 agglomerate behavior in SBR matrix were weakened obviously with

increasing the Sm-LDC content as displayed in Fig. 8d to 8f. This attributes to that the formation

of the hydrogen bonding and coordination bonding between the hydroxyl groups of the SiO_2 and

carboxyl group and samarium cation of Sm-LDC weakens effectively the strong polarity of SiO_2, resulting in the improvement of the compatibility between SiO_2 and SBR matrix[8,14,39,40]. It is worth noting that SiO_2 particles dispersed in rubber matrix homogeneously with using 6 phr Sm-LDC and no obvious improvement in dispersion states of SiO_2 is observed with further increasing Sm-LDC content.

3.6 Mechanical properties of SBR composites

The effect of Sm-LDC content on the mechanical properties of SBR/Sm-LDC/SiO_2 composites is compiled in Fig. 9. It can be seen that the tensile strength, elongation at break and tear strength of SBR/SiO_2 composites goes through a maximum at 6 phr Sm-LDC and then decreases with further increasing in Sm-LDC content. This is due to that the appropriate content of Sm-LDC can effectively promote a high crosslink density and well dispersion of SiO_2 in rubber matrix, as evidenced in the analysis of crosslink density and morphological observations. Although the high Sm-LDC content can produce more crosslink points, the excessive portion of Sm-LDC leads to more stress concentrations, thereby leading to the performance degradation. Surprisingly, the mechanical properties of SBR/Sm-LDC/SiO_2 are superior to those of SBR/Sm-LDC-0/SiO_2 composite even at low Sm-LDC content (1 phr). For SBR/Sm-LDC-6/SiO_2 composite, the tensile strength and tear strength are further enhanced to 23.63 MPa and 32.67 kN·m^{-1}, increasing by 164.9% and 39.4%, respectively, as compared with the SBR/Sm-LDC-0/SiO_2 composite. Such substantial improvements in mechanical properties of SBR/Sm-LDC/SiO_2 composites can be more clearly explained by the proposed model for the slippage and orientation of rubber chains in the filler-rubber interfacial region during stretching as described in Fig. 10. When an exerted stress is applied to the rubber matrix, the stress runs along the rubber chains and then the rubber chains are

stretched through slippage at low strain, as well as the slight deformation of filler agglomerates or particles as elliptical with the longest axis along the traction direction. Consequently, the stress concentration will lie in the two poles of the elliptical.[14,41,42] For the SBR/Sm-LDC-0/SiO$_2$ composite, on account of the serious agglomeration of SiO$_2$, small amounts of rubber chains are adsorbed around SiO$_2$ agglomerates and these chains are easy to slip off from the surface of SiO$_2$ agglomerates due to the weak filler-rubber interaction. Even worse, the SiO$_2$ agglomerates as stress concentrators also reduce the reinforcing efficiency of filler. As a result, decohesion will happen at the two poles of the elliptical and subsequently, the sample will destruct under a low tensile strength and strain as shown in Fig. 10a. In contrast, owing to the enhanced interfacial interaction between SiO$_2$ and rubber chains, much more rubber chains are restrained around the surface of SiO$_2$, and the stress will transfer to the filler effectively through hydrogen bonds and coordination bonds without decohesion in the SBR/Sm-LDC/SiO$_2$ composite. Meanwhile, the rubber chains can slip on the SiO$_2$ particles surface because the Sm-LDC acts as the soft multi-sulfur bonds, allowing the network to relax to a more perfect regime and changing the local stress condition by means of stress homogenized distribution. When the strain further increases, the SiO$_2$ particles will suffer a more severe deformation and the rubber chains stretched at low strain will not slip off from the surface of filler particles, and more stretched straight polymer chains with high orientation are formed as illuminated in Fig. 10b. Therefore, the process of the slippage and orientation of rubber chains, together with the deformation of SiO$_2$ particles distributes the stress evenly throughout the matrix and consumes huge sums of energy under stretching[42]. Thereinto, Sm-LDC molecules serve as "bridge" for a very efficient load transfer. All of these account for the great enhancement effect of Sm-LDC for mechanical properties of

SBR/Sm-LDC/SiO$_2$ composites.

3.7 Dynamic mechanical properties of SBR/Sm-LDC/SiO$_2$ composites

To further demonstrate the reinforcing efficiency of Sm-LDC on the performance of SBR/SiO$_2$ composites, DMA measurements were employed to study on dynamic mechanical properties. The dependency of storage modulus (E') and loss factor (tan δ) of SBR/Sm-LDC/SiO$_2$ composites and SBR/Sm-LDC-0/SiO$_2$ composite on temperature are displayed in Fig. 11a and 11b, respectively. The E' values of the composites can be regarded as a direct measure of the reinforcement effect of the filler which is very much dependent on the degree of filler dispersion and rubber-filler interfacial interaction.[43] A comparison of E' values among the SBR/Sm-LDC/SiO$_2$ composites reveals the maximum level for SBR/SiO$_2$ composite containing with 6 phr Sm-LDC. It is also notable that the E' values of SBR/Sm-LDC/SiO$_2$ composites show a significant improvement in comparison to SBR/Sm-LDC-0/SiO$_2$ composite, indicating that the compatibility and adhesion between the rubber matrix and SiO$_2$ particles are superior to those of SBR/Sm-LDC-0/SiO$_2$ composite, which is in accordance with the observation of morphology analysis and mechanical properties as discussed above. Meanwhile, tan δ of rubber composites can be calculated by the ratio of the viscous part to the elastic part (loss modulus/storage modulus), which can reflect how efficiently the material loses energy due to molecular rearrangements and internal friction. As shown in Fig. 11b, a glass transition region is observed in the curves of tan δ versus temperature. For that, the glass transition temperature (T$_g$) of the composites is obtained from the peak of the curve, as listed in Table 2. In comparison with SBR/Sm-LDC-0/SiO$_2$ composite, T$_g$ of SBR/Sm-LDC/SiO$_2$ composites is significantly shifted to a higher temperature with increasing Sm-LDC content, suggesting that the motion of the rubber molecular chains is restricted. This is

because the Sm-LDC can effectively facilitate the connection between the SiO_2 and rubber chains, finally resulting in that more rubber chains are immobilized onto the surface of SiO_2.

Noteworthily, skid resistance property and rolling resistance are two important parameters for high-performance rubber production (such as passenger tire), which can be evaluated by the tan δ at 0 °C and 60 °C, respectively. Nowadays, green tire materials with low rolling-resistance and high skid resistance has attracted tremendous attention in rubber industry, especially in SiO_2 reinforced rubber composite for the purpose of energy conservation, environmental protection, security and durability. But for the SiO_2 reinforced rubber composite, it always presents an opposite trend between rolling resistance and skid resistance. Accordingly, the ratio between tan δ at 0 °C and 60 °C can be used to assess the comprehensive dynamic properties for passenger tire tread rubber[44]. For SBR/Sm-LDC/SiO_2 composites, it is evident that the rolling resistance of SBR/Sm-LDC/SiO_2 composites is greatly reduced by the increasing content of Sm-LDC as shown in Table 2. When the content of Sm-LDC is up to 6 phr, rolling resistance is decreased by 45.3%, but with remaining almost unchanged in the skid resistance property. Furthermore, the rolling resistance and comprehensive dynamic properties of SBR/Sm-LDC-6/SiO_2 composite is about 56.0% lower and 79.0% higher than those of the SBR/Sm-LDC-0/SiO_2 composite, respectively. Hence, SBR/SiO_2 composite with appropriate content of Sm-LDC show a remarkable improvement in static and dynamic mechanical properties compared with these of SBR/Sm-LDC-0/SiO_2 composite. Such promising mechanical properties make SBR/Sm-LDC/SiO_2 composites very competitive for potential applications as the green tire materials.

4 Conclusions

RSC Advances Accepted Manuscript

In this study, a novel functionalized rare earth accelerator, samarium lysine dithiocarbamate (Sm-LDC), was successfully synthesized via the nucleophilic addition reaction between carbon disulfide and primary amine groups and the coordination reaction of samarium ions. Subsequently, the prepared Sm-LDC was utilized as multifunctional rubber agents to completely replace the conventional dithiocarbamate accelerator ZDC, activators ZnO and SA for preparing SBR/Sm-LDC/SiO$_2$ composites. The results demonstrated that Sm-LDC can observably accelerate the sulfur crosslinking reaction of both unfilled SBR compounds and SBR/SiO$_2$ compounds even without activator system (ZnO and SA). Sm-LDC not only promotes the dispersion of SiO$_2$ in the matrix, but also acts as bridge for reinforcing the filler-rubber interfacial interaction. Such phenomenon is responsible for the improved static and dynamic mechanical properties as compared with SBR/SiO$_2$ composite containing ZnO, SA and ZDC. For example, with adding 6 phr of Sm-LDC, tensile strength, and tear strength dramatically enhances to 23.63 MPa and 32.67 kN·m^{-1}, increased by 164.9% and 39.4%, respectively. Moreover, the rolling resistance of SBR/Sm-LDC-6/SiO$_2$ was reduced by 56.0 %, and simultaneously, the comprehensive dynamic property is promoted by 79.0%. Thus, SBR/Sm-LDC/SiO$_2$ composites exhibited very competitive for potential applications as the green tire materials. This study might expedite synthesis of the multi-functional rubber agents for enhancing rubber composites, and provides a new insight into the fabrication of high-performance rubber composites for engineering applications.

Acknowledgements

Rerference

1 R. Scotti, L. Wahba, M. Crippa, M. D' Arienzo, R. Donetti, N. Santo and F. Morazzoni, *Soft Matter.*, 2012, **8**, 2131-2143.

2 Y. Li, B. Y. Han, L. Liu, F. Z. Zhang , L. Q. Zhang, S. P. Wen, Y. L. Lu, H. B. Yang and J. Shen, *Compos. Sci. Technol.*, 2013, **88**, 69-75.

3 Z. H. Tang, Q. Y. Wei, T. F. Lin, B. C. Guo and D. M. Jia, *RSC Adv.*, 2013, **3**, 17057-17064.

4 B. C. Zhong, Z. X. Jia, Y. F. Luo, B. C. Guo and D. M. Jia, *Compos. Part A-Appl. S.*, 2015, **73**, 63-71.

5 M. Arroyo, M. A. López-Manchado and B. Herrero, *Polymer*, 2003, **44**, 2447-2453.

6 T. F. Lin, L. X. Zhu, W. W. Chen, S. W. Wu, B. C. Guo and D. M. Jia, *Appl. Surf. Sci.*, 2013, **280**, 888-897.

7 K. Sengloyluan, K. Sahakaro, W. K. Dierkes and J. W. M. Noordermeer, *Eur. Polym. J.*, 2014, **51**, 69-79.

8 B. C. Guo, F. Chen, Y. D. Lei, X. L. Liu, J. J. Wan and D. M. Jia, *Appl. Surf. Sci.*, 2009, **255**, 7329-7336.

9 Z. Gu, G. J. Song, W. S. Liu, P. Y. Li, L. Gao, H. H. Li and X. Hu, *Appl. Clay Sci.*, 2009, **46**, 241-244.

10 N. Rattanasom and S. Prasertsri, *Polym. Test.*, 2012, **31**, 645-653.

11 P. Rybiński, A. Pająk, G. Janowska and M. Jóźwiak, *J. Appl. Polym. Sci.*, 2015, **132**, 42593.

12 Y. Y. Yu, W. C. Chien and T. W. Tsai, *Polym. Test.*, 2010, **29**, 33-40.

13 E. Sumino, T. Saito, T. Noguchi and H. Sawada, *Polym. Adv. Technol.*, 2015, **26**, 345-352.

14 S. Y. Yang, L. Liu, Z. X. Jia, D. M. Jia and Y. F. Luo, *Polymer*, 2011, **52**, 2701-2710.

15 J. Travas-sejdic, J. Jelencic, M. Bravar and Z. Fröbe, *Eur. Polym. J.*, 1996, **32**, 1395-1401.

16 Y. Lin, Y. Z. Chen, Z. K. Zeng, J. R. Zhu, Y. Wei, F. C. Li and L. Liu, *Compos. Part A-Appl. S.*, 2015, **70**, 35-44.

17 P. J. Flory and J. Rehner, *J. Chem. Phys.*, 1943, **2**, 521-526.

18 P. J. Flory, *J. Chem. Phys.*, 1950, **18**, 108-111.

19 A. Tager, Physical Chemistry of Polymers, Cornell University Press, New York, 1953. p. 463.

20 E. Sathiyaraj, G. Gurumoorthy and S. Thirumaran, *NewJ. Chem.*, 2015, **39**, 5336-5349.

21 S. K. Verma and V. K. Singh, *J. Organomet. Chem.*, 2015, **791**, 214-224.

22 S. K. Singh, V. Kumar, M. G. B. Drewb and N. Singh, *Inorg. Chem. Commun.*, 2013, **37**,151-154.

23 P. Pitchaimani, K. M. Lo and K. P. Elango, *Polyhedron*, 2015, **93**, 8-16.

24 Y. Wei, S. L. Chen, F. C. Li, K.H. Liu and L. Liu, *Compos. Part A-Appl. S.*, 2015, **73**, 195-203.

25 B. Uno, N. Okumura, M. Goto and K. Kano, *J. Org. Chem.*, 2000, **65**, 1448-1455.

26 F. W. John and W. John, An introduction to surface analysis by XPS and AES. John Wiley & Sons Ltd, Chichester, England, 2003.

27 M. L. Du, B. C. Guo, Y. D. Lei, M. X.Liu and D. M. Jia, *Polymer*, 2008, **49**, 4871-4876.

28 Y. Zhang, M. Wang and J. Xu, *Mater. Sci. Eng. B-Adv.*, 1997, **47**, 23-27.

29 S. M. Hosseini and M. Razzaghi-Kashani, *Polymer*, 2014, **55**, 6426-6434.

30 S. Wollf, M. J. Wang and E. H. Tan, *Rubber. Chem. Technol.*, 1993, **66**,163-177.

31 S. Wollf, M. J. Wang and E. H. Tan, *KGK*, *Kautsch. Gummi Kunstst.*, 1994, **47**,102-107.

32 P. J. Nieuwenhuizen, A. W. Ehlers, J. G. Haasnoot, S. R. Janse, J. Reedijk and E. J. Baerends, *J. Am. Chem. Soc.*, 1999, **121**, 163-168.

33 P. J. Nieuwenhuizen, *Appl. Catal. A-Gen*., 2001, **207**, 55-68.

34 P. J. Nieuwenhuizen, A. W. Ehlers, J. W. Hofstraat, S. R. Janse, M. W. F. Nielen, J. Reedijk, and E.J. Baerends, *Chem. Eur. J*., 1998, **4**, 1816-1821.

35 M. Shumane, M. H. S. Gradwell and W. J. Mcgill, *J. Appl. Polym. Sci*., 2001, **82**, 3067-3073.

36 M. Shumane, M. H. S. Gradwell and W. J. Mcgill, *J. Appl. Polym. Sci*., 2001, **82**, 3074-3083.

37 S. Y. Yang, L. Liu, Z. X. Jia, D. M. Jia and Y. F. Luo, *J. Rare. Earth*., 2011, **29**, 444-453.

38 H. L. Peng, L. Liu, Y. F. Luo, X. P. Wang and D. M. Jia, *Polym. Compos*., 2009, **30**, 955-961.

39 B. C. Guo, F. Chen, Y. D. Lei and W. W. Chen, *Polym J*, 2010, **42**, 319-326.

40 B. C. Guo, Y. D. Lei, F. Chen, X. L. Liu, M. L. Du and D. M. Jia, *Appl. Surf. Sci*., 2008, **255**, 2715-2722.

41 E. Reynaud, T. Jouen, C. Gauthier, G. Vigier and J. Varlet, *Polymer*, 2001, **42**, 8759-8768.

42 A. N. Gent and B. Park, *J Mater Sci*., 1984, **19**, 1947-1956.

43 B. P. Kapgate and C. Das, *RSC Adv*., 2014, **4**, 58816-58825.

44 H. L. Peng, L. Liu, Y. F. Luo, H. Q. Hong and D. M. Jia, *J. Appl. Polym. Sci*., 2009, **112**, 1967-1973.
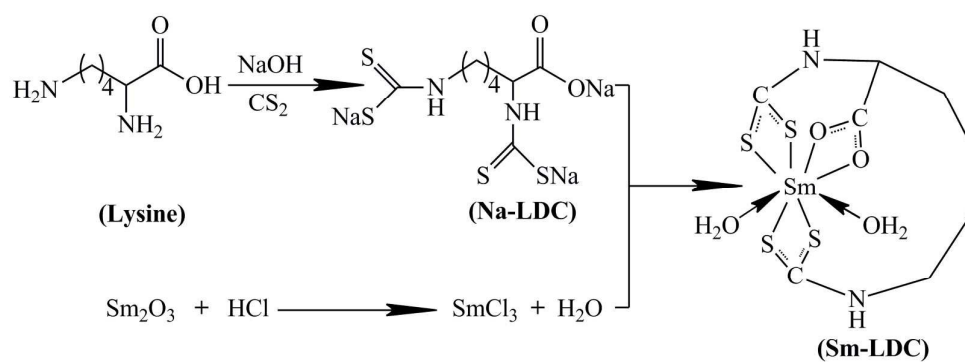
Fig. 1 Synthesis route of Sm-LDC.
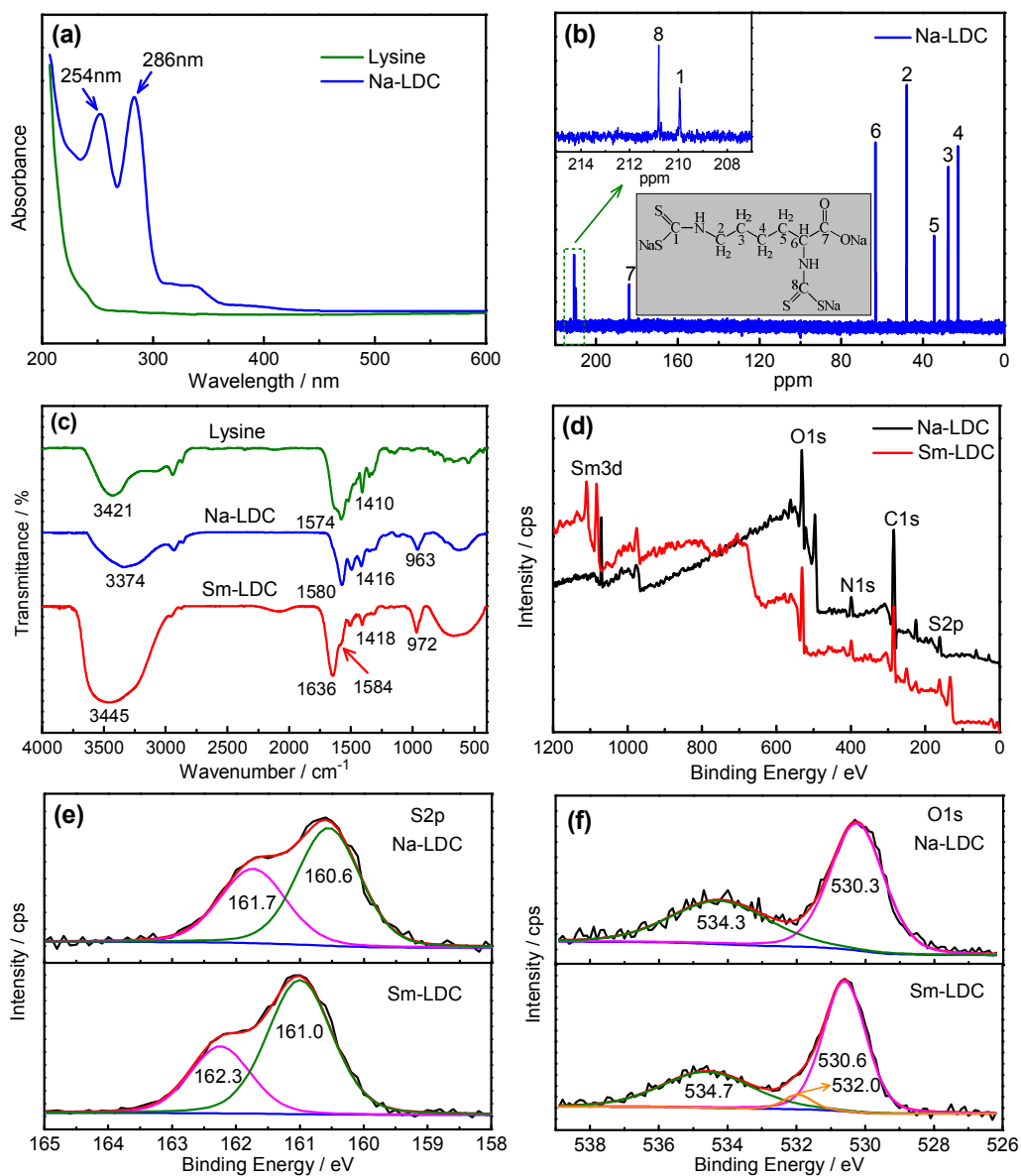
Fig. 2 UV-Vis absorption spectra of Lysine and Na-LDC (a), ^{13}C-NMR spectrum of Na-LDC (b), FT-IR spectra of Lysine, Na-LDC and Sm-LDC (c), the whole XPS spectra of Na-LDC and Sm-LDC (d), XPS S2p spectrums of Na-LDC and Sm-LDC (e), XPS O1s spectrums of Na-LDC and Sm-LDC (f).

25
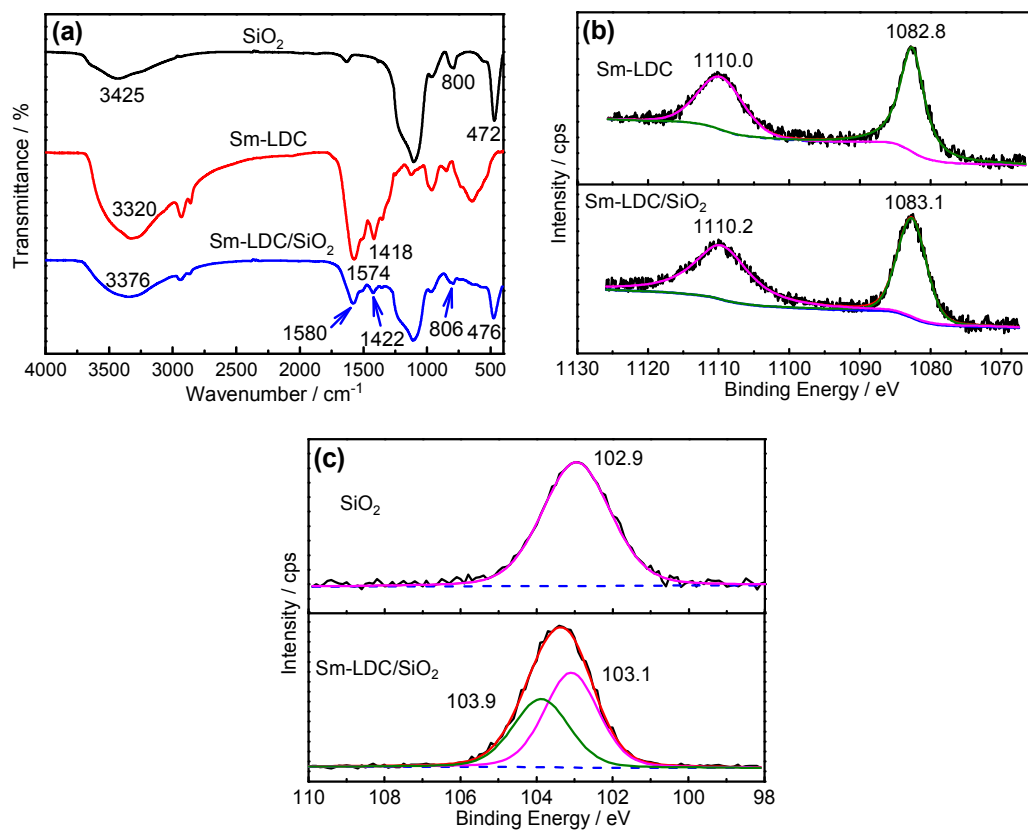
Fig. 3 FTIR spectra of SiO_2, Sm-LDC and Sm-LDC/SiO_2 model compounds (a); XPS Sm3d spectrums of Sm-LDC and Sm-LDC/SiO_2 model compounds (b); XPS Si2p spectrums of SiO_2 and Sm-LDC/SiO_2 model compounds.
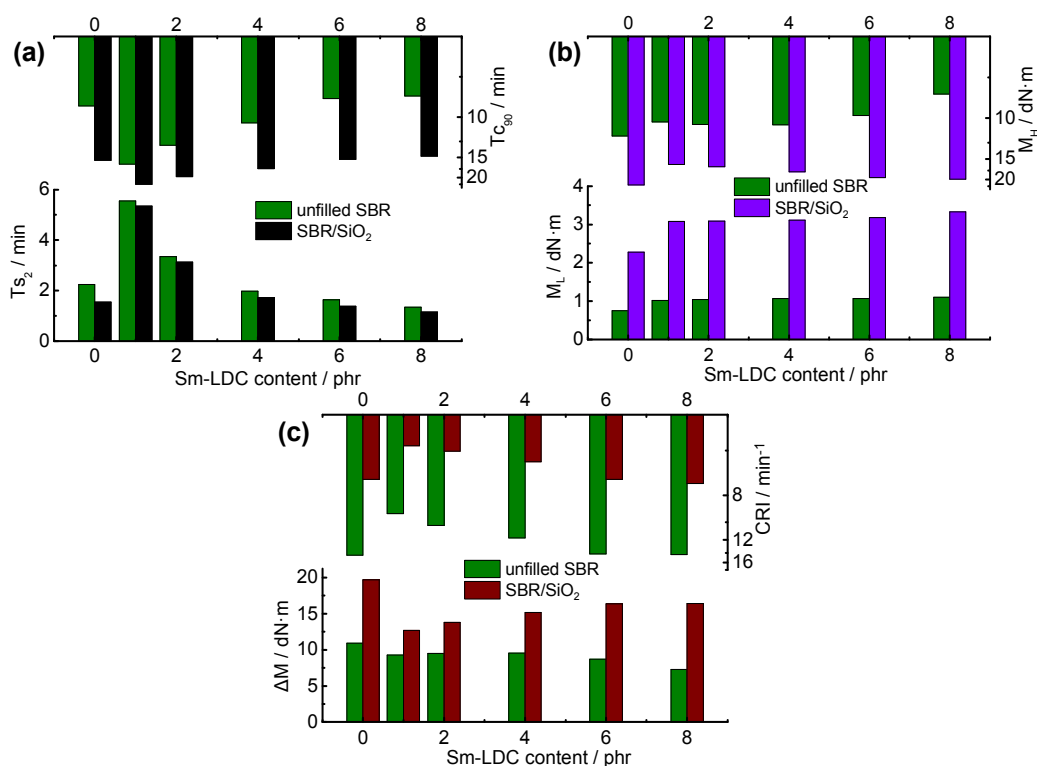
Fig. 4 Curing parameters of unfilled SBR and SBR/SiO$_2$ compounds: (a) Ts$_2$ and Tc$_{90}$; (b) M$_L$ and

M$_H$; (c) ΔM and CRI. The unfilled SBR and SBR/SiO$_2$ compounds with 0 phr Sm-LDC actually

refers to the unfilled SBR and SBR/SiO$_2$ compounds with 5 phr ZnO, 2 phr SA and 2 phr ZDC.
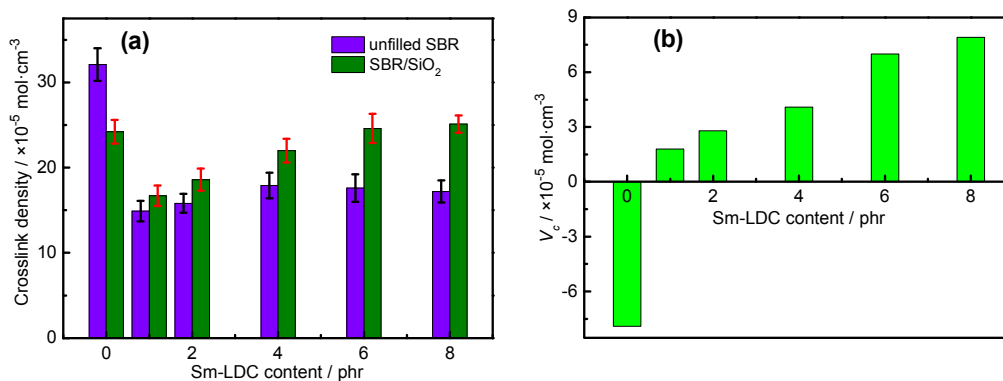
Fig. 5 Crosslink density of unfilled SBR and SBR/SiO$_2$ vulcanizates (a) and chemical crosslink of

filler-rubber interaction V_c (b). The unfilled SBR and SBR/SiO$_2$ vulcanizates with 0 phr Sm-LDC

actually refers to unfilled SBR and SBR/SiO$_2$ vulcanizates with 5 phr ZnO, 2 phr SA and 2 phr

ZDC.

27
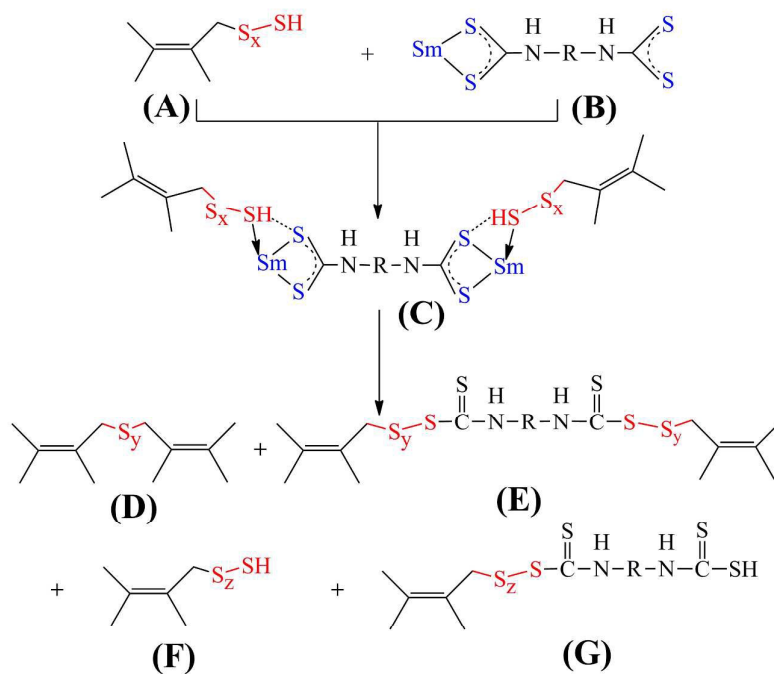
Note:R represents alkyl groups and carboxyl group in Sm-LDC

Fig. 6 Reaction process of vulcanization in SBR/Sm-LDC/SiO$_2$ compounds.
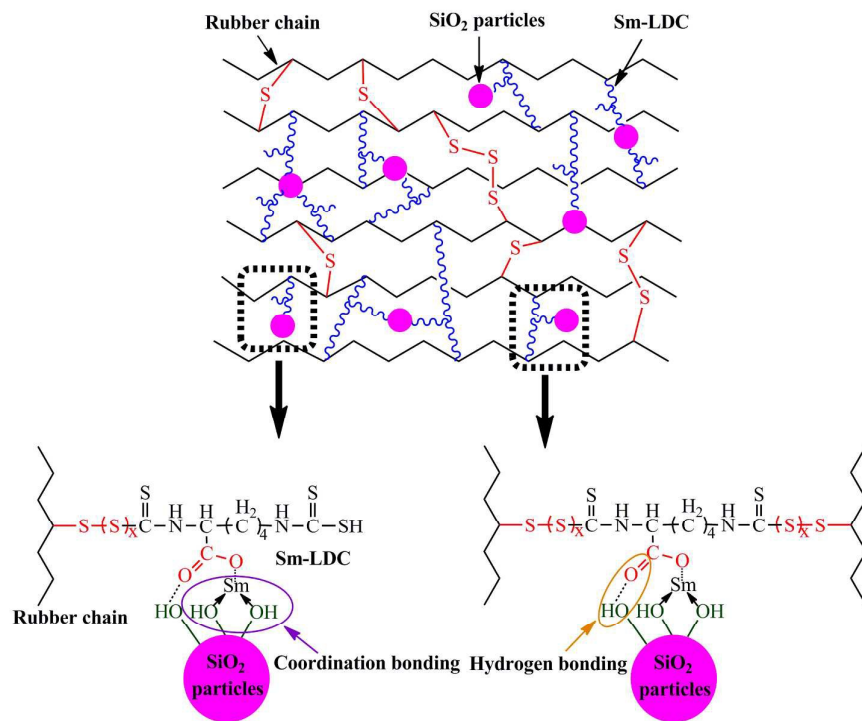
Fig. 7 Crosslink network in SBR/Sm-LDC/SiO$_2$ composites.

28
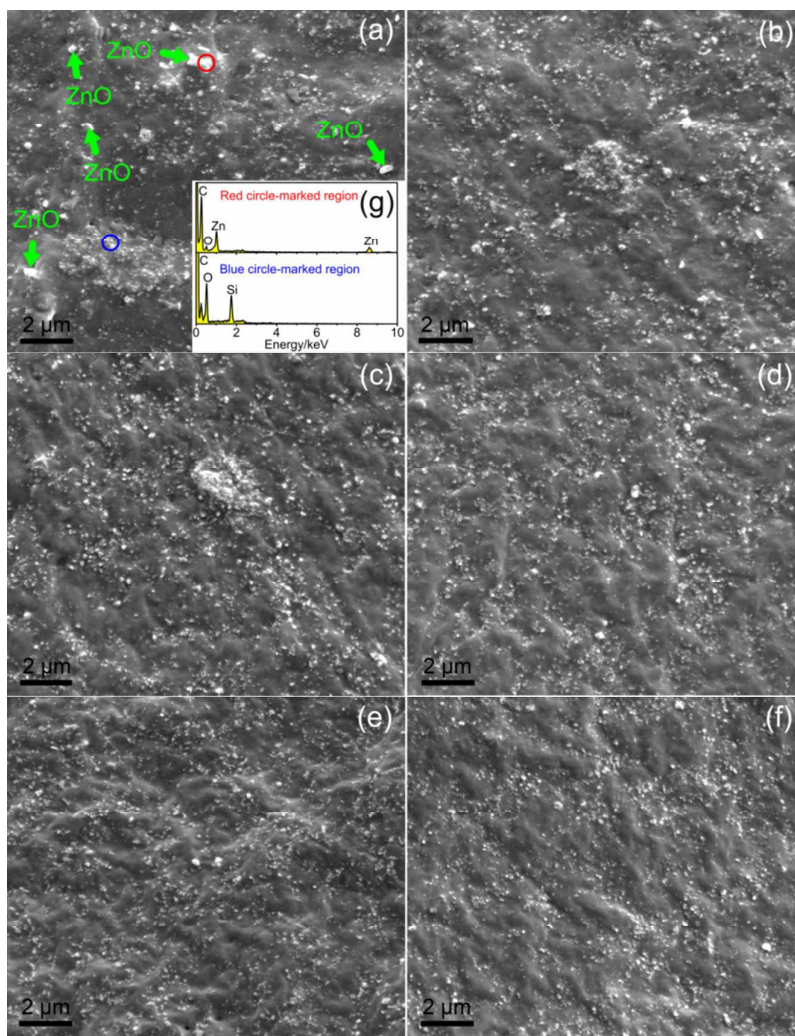
Fig. 8 FESEM images of SBR/SiO$_2$ composites with 5 phr ZnO, 2 phr SA and 2 phr ZDC (a); 1

phr Sm-LDC (b); 2 phr Sm-LDC (c); 4 phr Sm-LDC (d); 6 phr Sm-LDC (e); 8 phr Sm-LDC (f)

and EDS spectra of the corresponding circle-marked region in SBR/SiO$_2$ composite with 5 phr

ZnO, 2 phr SA and 2 phr ZDC (g).
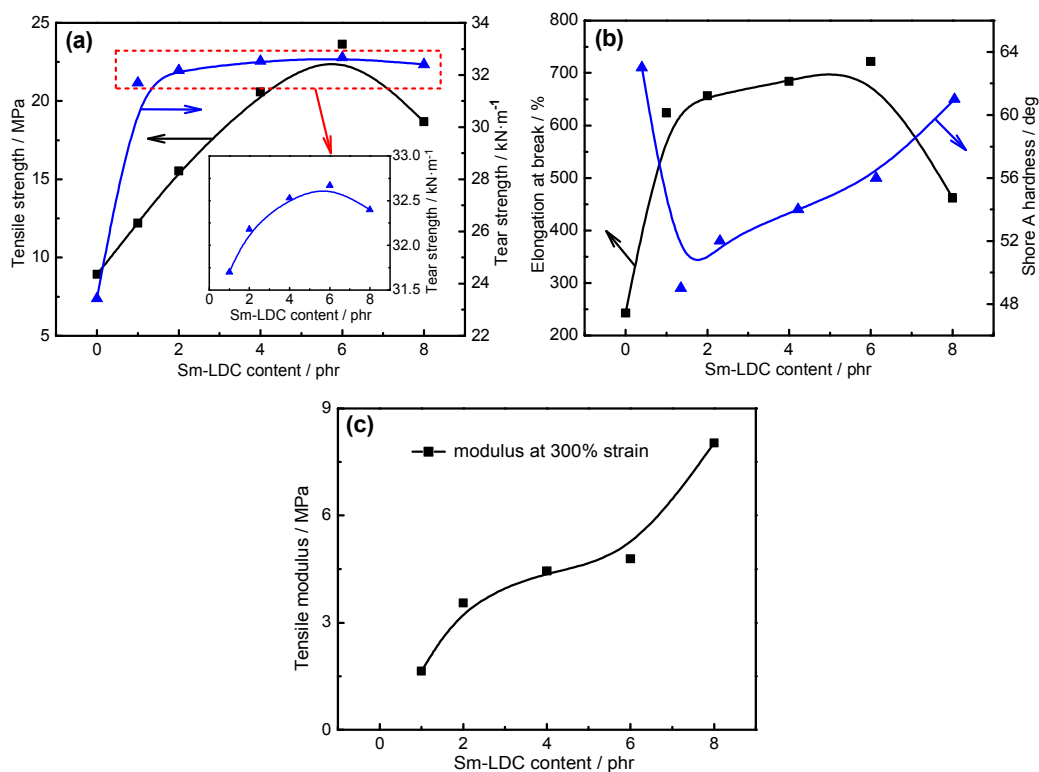
Fig. 9 Mechanical properties of SBR/Sm-LDC/SiO$_2$ composites: (a) tensile strength and tear strength; (b) elongation at break and Shore A hardness; (c) Modulus at 300% strain. The SBR/Sm-LDC-0/SiO$_2$ composite actually refers to the SBR/SiO$_2$ composite with 5 phr ZnO, 2 phr SA and 2 phr ZDC.
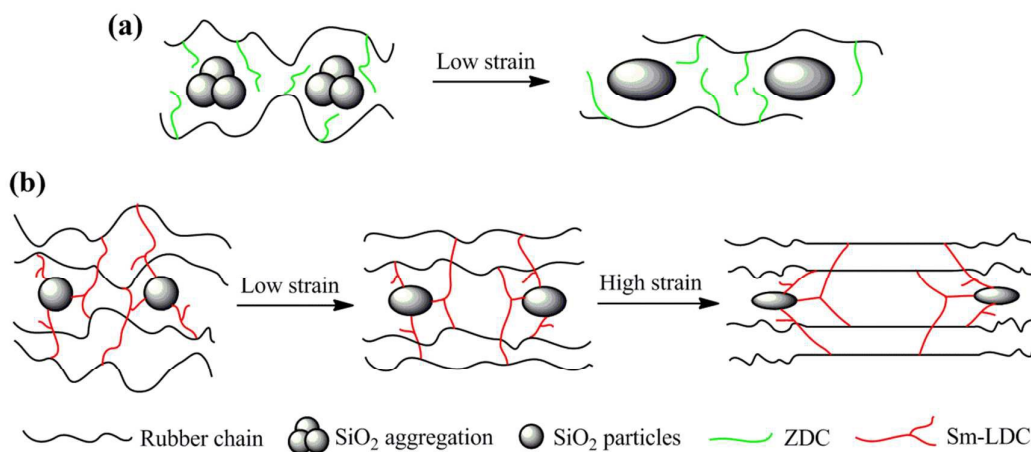
Fig. 10 Proposed model of the reinforcement mechanism of Sm-LDC in SBR/Sm-LDC/SiO$_2$ composites.
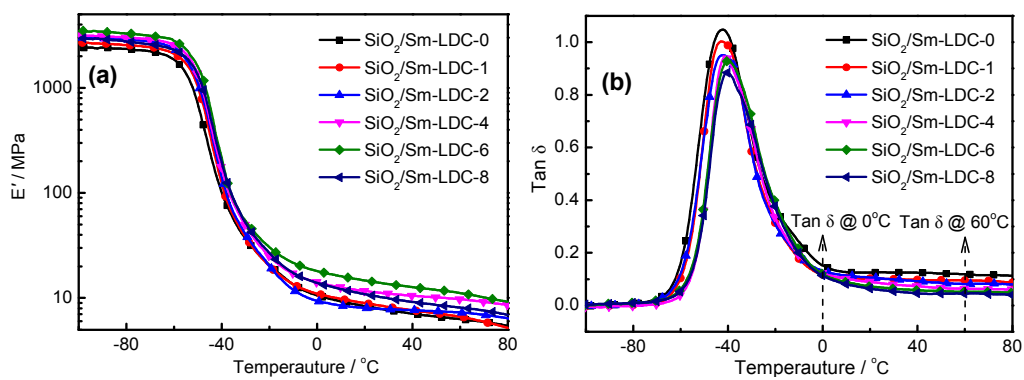
Fig. 11 Temperature dependence of the storage modulus (a) and the loss factor (b) of SBR/Sm-LDC-0/SiO$_2$ composite and SBR/Sm-LDC/SiO$_2$ composites. The SBR/Sm-LDC-0/SiO$_2$ composite actually refers to the SBR/SiO$_2$ composite with 5 phr ZnO, 2 phr SA and 2 phr ZDC.

Table 1 element content of Sm-LDC.

Element content	N%	C%	H%
Experimental values	5.69	19.81	3.25
Theoretical values	5.82	19.96	3.12

Table 2 Summary of DMA results of SBR/Sm-LDC-0/SiO$_2$ composite and SBR/Sm-LDC/SiO$_2$ composites with different Sm-LDC contents.

Samples	T$_g$ / °C	Tan δ/0 °C	Tan δ/60 °C	Ratio, 0 °C/60 °C
SiO$_2$/Sm-LDC-0[a]	-42.3	0.151	0.118	1.28
SiO$_2$/Sm-LDC-1	-42.8	0.117	0.095	1.23
SiO$_2$/Sm-LDC-2	-42.1	0.132	0.082	1.61
SiO$_2$/Sm-LDC-4	-41.3	0.123	0.063	1.95
SiO$_2$/Sm-LDC-6	-40.1	0.119	0.052	2.29
SiO$_2$/Sm-LDC-8	-40.5	0.110	0.050	2.20

[a]The SBR/Sm-LDC-0/SiO$_2$ composite actually refers to the SBR/SiO$_2$ composite with 5 phr ZnO, 2 phr SA and 2 phr ZDC.

Graphical abstract